

## Structural, Optical and Electrical Properties of Ce Doped SnO<sub>2</sub> Nanoparticles Prepared by Surfactant Assisted Gel Combustion Method

M. Veerabhadrayya<sup>1</sup>, R. Ananda Kumari<sup>2</sup>, G. Nagaraju<sup>3</sup>, Udayabhanu<sup>3</sup>, Y.T. Ravikiran<sup>4</sup>, B. Chethan<sup>5</sup>

<sup>1</sup> University College of Science, Tumkur University, 572103 Tumakuru, India

<sup>2</sup> Shri Siddaganga College of Arts, Science and Commerce, 572102 Tumakuru, India

<sup>3</sup> Energy Materials Research Laboratory, Department of Chemistry,  
Siddaganga Institute of Technology, 572103 Tumakuru, India

<sup>4</sup> Department of PG Studies in Physics, Government Science College, 577501 Chitradurga, India

<sup>5</sup> Visvesvaraya Technological University, 590018 Belagavi, India

(Received 01 April 2020; revised manuscript received 15 August 2020; published online 25 August 2020)

Nanocrystalline pure and Ce doped tin oxide (SnO<sub>2</sub>) powders were synthesized through surfactant (CTAB and PEG) assisted gel combustion method using urea as a fuel. Prepared samples were characterized by PXRD, FESEM, UV-Vis, FTIR and Impedance analyzer. The PXRD analysis revealed the tetragonal rutile SnO<sub>2</sub> phase. The grain size was estimated using the Debye-Scherrer equation and Williamson-Hall method. The cell parameters were found using Rietveld refinement and Nelson-Riley plot method. The FESEM pictures showed the formation of nanoparticles of almost spherical shape. FTIR spectrum revealed the bands due to the fundamental overtones and combination of Sn-O and Sn-O-Sn entities. The UV-Vis spectra showed the decrease in band gap with Ce content due to an increase in defects. The effect of Ce doping on the electrical properties was studied at room temperature. The dielectric parameters,  $\epsilon'$  and  $\tan\delta$  were maximum for pure SnO<sub>2</sub> sample. The variation of dielectric properties and ac conductivity with frequency is due to the Maxwell-Wagner type of interfacial polarization.

**Keywords:** Tin oxide, Gel combustion method, Rietveld refinement, Ac conductivity.

DOI: [10.21272/jnep.12\(4\).04017](https://doi.org/10.21272/jnep.12(4).04017)

PACS numbers: 61.46.Df, 73.63.Bd,  
77.22.Gm, 78.67.Bf,

### 1. INTRODUCTION

Nanoscale semiconducting oxides are of significant interest due to their applications. Tin oxide (SnO<sub>2</sub>) is a versatile semiconducting material for many applications such as optoelectronic devices, gas sensors, dye based solar cells and secondary lithium batteries due to its wide band gap of 3.6 eV at 300 K, large excitation binding energy and good optical transparency in the visible region [1, 2]. The incorporation of additives into SnO<sub>2</sub> introduces surface defects thereby, alters its structure and grain size [3]. Doping of Ce improves the dielectric response and ac conductivity in metal oxide semiconductors [4]. The addition of surfactants controls the free energy of the surface and, therefore, the reactivity of the particles [5]. Several methods of synthesizing nanoparticles have been reported [1-6]. Here we have reported the study of structural, optical and electrical properties of Ce doped SnO<sub>2</sub> nanoparticles prepared by surfactants cetyl trimethylammonium bromide (CTAB) and polyethylene glycol (PEG) assisted gel combustion method using urea as a fuel.

### 2. EXPERIMENTAL

The AR grade chemicals tin (II) chloride dihydrate [SnCl<sub>2</sub>.2H<sub>2</sub>O], nitric acid [HNO<sub>3</sub>], urea [CH<sub>4</sub>N<sub>2</sub>O] (Sd Fine Chem Ltd.), CTAB [C<sub>19</sub>H<sub>42</sub>BrN], PEG (C<sub>2</sub>H<sub>4</sub>O)<sub>n</sub>H<sub>2</sub>O (Loba Chemie Pvt. Ltd.) and cerium nitrate [Ce(NO<sub>3</sub>)<sub>3</sub>] (Sigma-Aldrich) were used without further purification. Deionized water was used during preparation.

Pure and Ce doped tin oxide (SnO<sub>2</sub>) nanocrystalline powders were synthesized by surfactant assisted gel combustion method using urea as a fuel. Stoichiometric amount of tin (II) chloride dihydrate, urea and cerium

nitrate (0.00, 0.02, 0.04, 0.06, 0.08 and 0.1 mole %) were mixed in deionized water taken in a beaker and placed on a magnetic stirrer with hot plate. To this mixture 0.1 M of CTAB and 1 mL of PEG was added, and dilute nitric acid (1:1) was added till the mixture becomes transparent. When this mixture was stirred for 15 min at 100 °C, gel was formed. Then the mixture was transferred to a muffle furnace at 400 °C where the gel underwent a combustion reaction with evolution of gases and tin oxide powder was formed. The powders produced were then calcinated at 800 °C for 3 h.

The structural characterization was performed using Rigaku powder X-ray diffractometer (PXRD) with CuK $\alpha$  (1.54056 Å) radiation. The morphology was studies using field emission scanning electron microscope (Carl ZEISS SIGMA). FTIR spectrum of the samples was taken with Perkin-Elmer spectrometer. Electrical properties were studied using HIOKI 3532-50 LCR HiTESTER.

### 3. RESULTS AND DISCUSSION

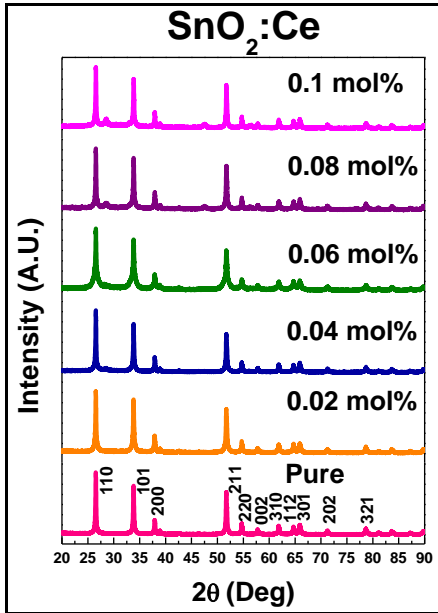
#### 3.1 PXRD Studies

Fig. 1 shows the PXRD patterns of SnO<sub>2</sub> samples. The reflections are consistent with a tetragonal rutile structure with space group P42/mnm (JCPDS No. 41-1445).

The mean crystallite size ( $D$ ) of the nanoparticles was estimated using the Debye-Scherrer formula

$$D = K\lambda / \beta \cos\theta, \quad (1)$$

where  $K$  is the shape factor (~ 0.9),  $\lambda$  is the wavelength of X-ray radiation used (= 0.154056 nm),  $\beta$  is the angular peak width at half maximum (FWHM) intensity and  $\theta$  is the Bragg angle.



**Fig. 1** – PXRD pattern of pure and Ce doped  $\text{SnO}_2$  nanopowders

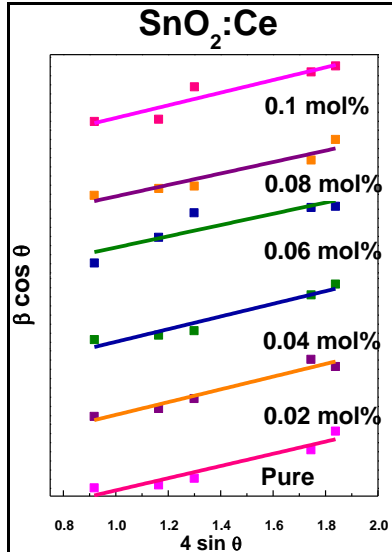


**Fig. 2** – W-H analysis for pure and Ce doped  $\text{SnO}_2$  nanopowders

The X-ray diffraction pattern shows line broadening because of particle size and strain. The line broadening is described by Williamson-Hall (W-H) equation [6]:

$$\beta \cos \theta = (0.94\lambda / D) + 4\varepsilon \sin \theta, \quad (2)$$

where  $\varepsilon$  is the strain,  $\beta$  is the instrumental broadening. The average crystallite size  $D$  and strain  $\varepsilon$  were computed using the least squares method. W-H plots with  $4\sin\theta$  on the  $x$ -axis and  $\beta \cos \theta$  on the  $y$ -axis are shown in Fig. 2.

The particle size  $D$  and strain  $\varepsilon$  are calculated from the  $y$ -intercept and slope, respectively. The calculated values of the crystallite size  $D$  are shown in Table 1.

The dislocation density ( $\delta$ ) is calculated from the Williamson and Smallman's formula [7]

$$\delta = \frac{n}{D^2}, \quad (3)$$

where  $n$  is a factor which when equal to unity gives the minimum dislocation density, and  $D$  is the average crystallite size. The dislocation densities for the prepared tin oxide nanoparticles are shown in Table 1.

**Table 1** – Crystallite size, lattice strain and dislocation density of pure and Ce doped  $\text{SnO}_2$  nanopowders

Ce concentration (%)	Crystallite size (nm)		Lattice strain $\varepsilon (10^{-4})$	Dislocation density ( $10^{14} \text{ m}^{-2}$ )
	Debye-Scherrer	W-H plot		
0.00	42.89	40.31	8.15	5.43
0.02	41.97	40.42	8.44	5.68
0.04	40.65	36.58	8.75	6.05
0.06	37.62	32.39	9.64	7.07
0.08	44.02	39.39	7.98	5.16
0.10	43.90	38.51	8.05	5.19

To determine the accurate values of cell parameters Nelson-Riley plot method and Rietveld refinement method were used.

### a) Nelson-Riley Plot

The lattice parameters  $a$  and  $c$  of  $\text{SnO}_2$  nanopowders with a tetragonal structure were corrected using the Nelson-Riley plot. The distance between the diffraction planes  $d$  of  $\text{SnO}_2$  was calculated from the Bragg equation

$$2d \sin \theta = n\lambda \quad (4)$$

and the tetragonal lattice parameter ( $a = b \neq c$ ) for the tetragonal phase structure was determined by the equation

$$\frac{1}{d^2} = \frac{h^2 + k^2}{a^2} + \frac{l^2}{c^2}. \quad (5)$$

The corrected values of the lattice parameters were estimated from the Nelson-Riley plots shown in Fig. 3 [8]. The calculated lattice parameters for different planes were plotted versus error function

$$f(\theta) = \frac{\cos^2 \theta}{\sin \theta} + \frac{\cos^2 \theta}{\theta}. \quad (6)$$

The intercepts of the plots give lattice parameters  $a$  and  $c$ .

### b) Rietveld Refinement

The PXRD patterns of pure and Ce doped  $\text{SnO}_2$  nanopowders were analyzed by the Rietveld technique using the FULLPROF Suite program [9]. Fig. 4a depicts the observed, calculated and difference PXRD profiles for Ce doped  $\text{SnO}_2$  nanoparticles (6 mol. %). It can be seen that the profiles for observed and calculated ones match. The unit cell structure of  $\text{SnO}_2$  nanoparticles was shown in Fig. 4b.

During refinement, the parameters such as occupancies, lattice constants, shape parameters, scale factors and oxygen positions were taken as free parameters. The atomic positions for tin were fixed. Isothermal parameters were fixed for both tin and oxygen. Background was fitted with a sixth-order polynomial and the peak shapes were described by pseudo-Voigt profiles.

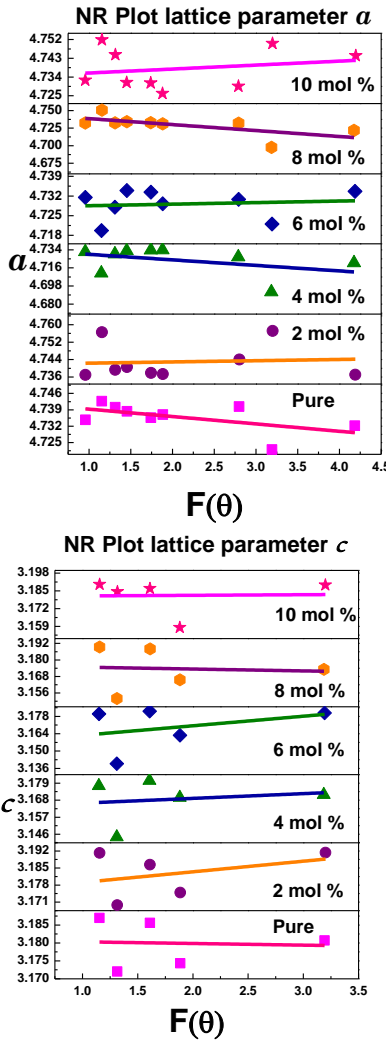
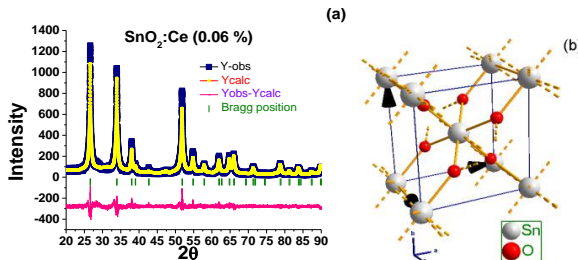
Fig. 3 – NR plots of the lattice parameters  $a$  and  $c$ Fig. 4 – (a) Rietveld refinement plot; (b) unit cell structure of Ce doped  $\text{SnO}_2$  (6 mol. %)

Table 2 – Values of lattice parameters

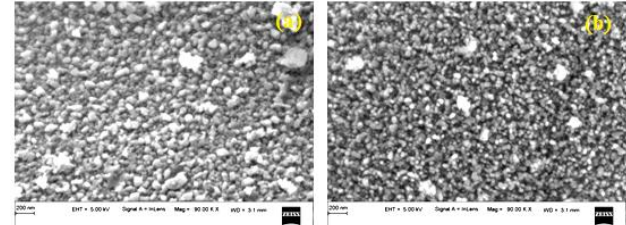
Ce concentration	Lattice parameter*			
	$a$		$c$	
	Rietveld refinement	NR plot	Rietveld Refinement	NR plot
Pure	4.737	4.742	3.186	3.181
0.02 %	4.736	4.742	3.186	3.175
0.04 %	4.736	4.735	3.186	3.163
0.06 %	4.737	4.728	3.186	3.155
0.08 %	4.736	4.747	3.186	3.176
0.10 %	4.736	4.734	3.185	3.181

\* Standard values (JCPDF No. 41-1445):  $a = 4.7382$  and  $c = 3.1871$ 

Table 2 shows the values of lattice parameters obtained from Rietveld refinement and Nelson-Riley plots.

### 3.2 Field Emission Scanning Electron Microscopy (FESEM)

Fig. 5 shows the morphologies of pure and Ce doped  $\text{SnO}_2$  samples. The images show that the samples comprise of crystalline nanosized grains with almost spherical morphology. The agglomeration may be due to surface tension and interactive forces [10].

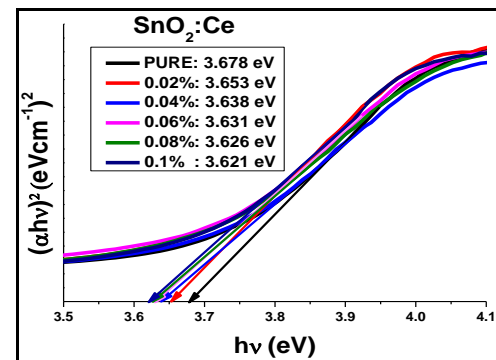
Fig. 5 – SEM micrographs of (a) pure and (b) Ce doped  $\text{SnO}_2$  nanoparticles (6 mol. %)

### 3.3 UV-Vis Analysis

UV-Vis spectra of  $\text{SnO}_2$  samples were recorded in the wavelength range 200-800 nm. Fig. 6 shows the Tauc's plot of  $\text{SnO}_2$  samples. Optical band gap of the nanoparticles was determined from the intercept on the  $x$ -axis obtained by extrapolating the linear part of the Tauc's plot. The Tauc's relation is given by equation [11]

$$(\alpha h\nu)^n = A(h\nu - E_g), \quad (7)$$

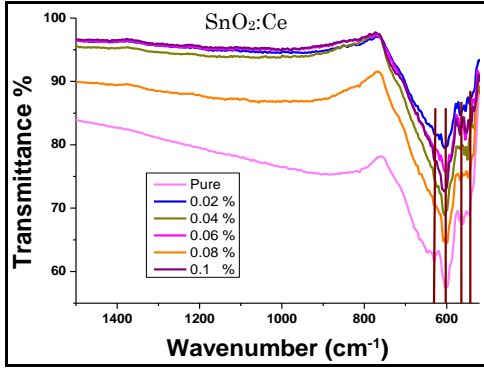
where  $E_g$  is the optical band gap,  $h$  is the Planck constant and  $\nu$  is the frequency of incident photons,  $A$  is a band tailing parameter, and  $n$  is the index ( $= 2$  for the indirect allowed transitions). The band gap values of undoped and doped samples from Tauc's plots come out to be in the range 3.678-3.621 eV. The gradual decrease in the band gap with Ce content may be due to the substitution of Ce ions for Sn sites. This can also be due to an increase in the number of defects [12].

Fig. 6 – Plots of  $(\alpha h\nu)^2$  against  $h\nu$  of Ce doped  $\text{SnO}_2$  nanoparticles

### 3.4 FTIR Analysis

FTIR is a technique used to obtain information regarding bonding and functional groups in a material. The band positions and numbers of absorption peaks depend on the crystalline structure, chemical composition,

and also on morphology [13]. FTIR analysis was carried out at room temperature over the wave number range of 400-4000 cm<sup>-1</sup>. The FTIR transmittance spectra of the undoped and Ce doped SnO<sub>2</sub> nanoparticles are presented in Fig. 7. The very strong absorption bands were observed in the range 540-630 cm<sup>-1</sup> which were attributed to the Sn-O antisymmetric vibrations. In that region, the peak at 602 cm<sup>-1</sup> is assigned to Sn-O-Sn vibrations. The bands exhibited at 541, 563 and 629 cm<sup>-1</sup> are attributed to the Sn-O stretching vibrations [1, 12].



**Fig. 7** – FTIR spectra of the undoped and Ce doped SnO<sub>2</sub> nanoparticles

### 3.5 Electrical Properties Study

The SnO<sub>2</sub> nanopowders were pressed into pellets of 13 mm diameter and 1 mm thickness and coated on adjacent faces with silver paste for electrical measurements. Dielectric and impedance spectroscopy measurements were carried out in the frequency range 5 Hz to 5 MHz using Hioki 3532-50 LCR HiTester.

The dielectric constant is represented by

$$\epsilon = \epsilon' - i\epsilon'' . \quad (8)$$

The first term is the real part of the dielectric constant which describes the stored energy, while the second term is the complex dielectric constant which describes the dissipated energy.

The value of the real part of the dielectric constant  $\epsilon'$  of the samples was calculated using the formula

$$\epsilon' = \frac{C_p d}{\epsilon_0 A} , \quad (9)$$

where  $\epsilon_0$  ( $\sim 8.85 \times 10^{-12}$  F·m<sup>-1</sup>) is the permittivity of free space,  $d$  is the thickness of the pellet,  $A$  is the cross sectional area of the flat surface of the pellet, and  $C_p$  is the capacitance of the specimen in Farad (F).

The complex dielectric constant  $\epsilon''$  of the samples was calculated using the relation

$$\epsilon'' = \epsilon' \tan \delta , \quad (10)$$

where  $\tan \delta$  is the dielectric loss tangent proportional to the loss of energy from the applied field into the sample.

The variation of the real part of the dielectric constant  $\epsilon'$  with frequency for the SnO<sub>2</sub> samples is shown in Fig. 8.

The dielectric constant decreases with increasing frequency of the applied field and becomes almost

frequency independent at high frequencies. This can be explained on the basis of Maxwell-Wagner model [14]. According to this model, the dielectric medium is made of well conducting grains with poorly conducting grain boundaries. On the application of an external electric field, the charge carriers will be accumulated at the grain boundaries. This causes large polarization and results in high dielectric constant. The polarization decreases with the increase in frequency and then reaches a constant value since the hopping between metal ions cannot follow the alternating field. It has also been observed that the value of the dielectric constant is more for the doped samples due to high polarizability of cerium ions as compared to tin [15].

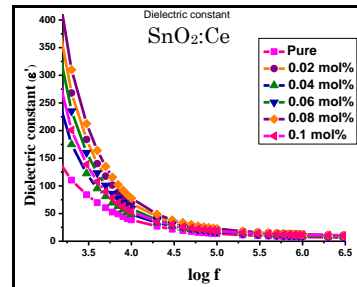


**Fig. 8** – Frequency dependent variation of dielectric constant

Dielectric loss represents the energy dissipation in the dielectric system. Fig. 9 shows the variation of dielectric loss with frequency at room temperature. At lower frequencies, the value of  $\tan \delta$  is large for pure SnO<sub>2</sub> sample due to the dominant effect of the polarization by migrating charges at low frequency.

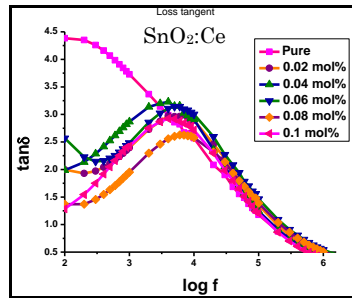


**Fig. 9** – Frequency dependent variation of dielectric loss

Higher dielectric loss is observed at lower frequencies due to space charge polarization which can be explained through the Shockley-Read mechanism [16]. According to this mechanism, at low and middle order frequencies the impurity ions in the bulk crystal matrices capture the surface electron resulting in space charge polarization at the surface. The dielectric loss increases from lower to higher frequencies till a relaxation peak is observed at middle frequencies and then decreases with further increase in frequency.

When the jumping frequency of localized electric field carriers is approximately equal to the external applied field, then relaxation peaks are observed at the middle frequencies.

The ac conductivity of the samples is evaluated by using the following expression:

$$\sigma_{AC} = \epsilon' \epsilon_0 \omega \tan \delta . \quad (11)$$

The ac conductivity is related to the dielectric relaxation caused by the localized electric charge carriers and obeys empirical power law [17]

$$\sigma(\omega) = A\omega^s, \quad (12)$$

where  $A$  is the complex proportionality constant and  $s$  represents the temperature dependent parameter whose value is less than unity. Fig. 10 shows the variation of  $\sigma_{AC}$  with frequency. The ac conductivity at low frequencies increases slowly but at higher frequencies there is a sharp increase in the conductivity. This can be explained by hopping model [18] according to which the increase in frequency of the applied field increases the hopping of charges between the charge carriers  $\text{Sn}^{4+}$  and  $\text{Sn}^{2+}$  which causes an increase in the mobility of charge carriers and the conductivity.

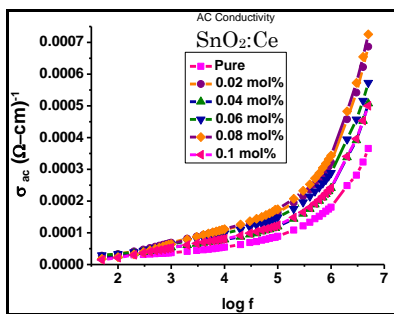


Fig. 10 – Frequency dependent variation of ac conductivity

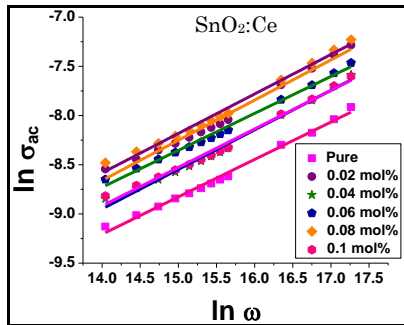


Fig. 11 – Dependence of  $\ln \sigma_{AC}$  on  $\ln \omega$

## REFERENCES

- S.A. Saleh, A.A. Ibrahim, S.H. Mohamed, *Acta Phys. Pol. A.* **129**, 1220 (2016).
- Taehee Kim, Vinayak G. Parale, Hae-Noo-Ree Jung, Younghun Kim, Zied Driss, Dorra Driss, Abdallah Bouabidi, Souhir Euchy, Hyung-Ho Park, *Nanomaterials* **2019**, 358 (2019).
- Yuan-Chang Liang, Chia-Min Lee, Ya-Ju Lo, *RSC Adv.* **7**, 4724 (2017).
- Jasneet Kaur, Vinay Gupta, R K Kotnala, Kuldeep Chand Verma, *Indian J. Pure Appl. Phys.* **50**, 57 (2012).
- Salwa, M.I. Morsy, *Int. J. Curr. Microbiol. App. Sci.* **3**, 5 (2014).
- N. Bhakta, P.K. Chakrabarti, *Appl. Phys. A-Mater.* **125**, 73 (2019).
- G.K. Williamson, R.E. Smallman, *Philos. Mag.* **1**, 34 (1956).
- Simin Tazikeh, Amir Akbari, Amin Talebi, Emad Talebi, *Mater. Sci-Poland.* **32**, 98 (2013).
- J. Rodríguez-Carvajal, *Phys. B Condens. Matter* **192**, 55 (1993).
- G. Inci, A. Arnold, A. Kronenburg, R. Weeber, *Aerosol Sci. Tech.* **48**, 842 (2014).
- Feroz A. Mir, *Result. Phys.* **4**, 103 (2014).
- Ateeq Ahmed, M. Naseem Siddique, T. Ali, P. Tripathi, *Appl. Surf. Sci.* **483**, 463 (2019).
- M. Ashokkumar, S. Muthukumaran, *Superlatt. Microstruct.* **69**, 53 (2014).
- Sumaira Mehraj, M. Shahnawaze Ansari, Alimuddin, *J. Nano-eng. Nanomanuf.* **3**, 229 (2013).
- N.K. Divya, P.U. Aparna, P.P. Pradyumnan, *Adv. Mater. Phys. Chem.* **5**, 287 (2015).
- W. Shockley, W.T. Read, *Phys. Rev.* **87**, 835 (1952).
- A. Oueslati, F. Hlel, K. Guidara, M. Gargouri, *J. Alloy. Compd.* **492**, 508 (2010).
- S. Mahalakshmi, K.S. Manja, *J. Alloy. Compd.* **457**, 522 (2008).
- Sumaira Mehraj, M. Shahnawaze Ansari, Alimuddin, *Physica B* **430**, 106 (2013).

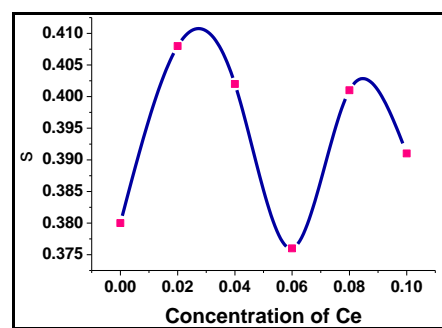


Fig. 12 – Variation of exponent  $s$  with concentration of Ce

Fig. 11 shows the plot of  $\ln \sigma_{AC}$  versus  $\ln \omega$  for Ce doped  $\text{SnO}_2$  nanoparticles according to Eq. (12).

Fig. 12 shows the variation of exponent  $s$  with Ce concentration which was calculated with the help of Fig. 10. The value of  $s$  lies between 0.38 and 0.408 which suggests that the conduction phenomenon in the studied samples follows hopping model [19].

## 4. CONCLUSIONS

Pure and Ce doped tin oxide ( $\text{SnO}_2$ ) nanocrystalline powders were prepared successfully through surfactant assisted gel combustion method. The tetragonal rutile  $\text{SnO}_2$  phase of the samples was confirmed by the PXRD analysis. The grain sizes estimated are in the range 32-44 nm. The values of the cell parameters found using Rietveld refinement and Nelson-Riley plot method are comparable. The formation of almost spherical nanoparticles is seen from FESEM pictures. FTIR spectrum confirmed the presence of Sn-O bond. Ce doping introduced the defects in the host which is confirmed in UV-Vis analysis by decrease in bandgap. The decrease in the dielectric constant with frequency is attributed to the Maxwell-Wagner type of interfacial polarization. The value of the dielectric constant is more for doped samples due to high polarizability of cerium ions as compared to tin ones. The higher dielectric loss observed at lower frequencies is due to Shockley-Read mechanism. Also we can observe the dielectric relaxation peaks. The ac conductivity study revealed hopping-type conduction in the samples. Frequency-dependent ac conductivity obeys the power law.

**Структурні, оптичні та електричні властивості легованих Ce наночастинок SnO<sub>2</sub>, підготовлених методом горіння гелю з додаванням поверхнево-активних речовин**

M. Veerabhadrayya<sup>1</sup>, R. Ananda Kumari<sup>2</sup>, G. Nagaraju<sup>3</sup>, Udayabhanu<sup>3</sup>, Y.T. Ravikiran<sup>4</sup>, B. Chethan<sup>5</sup>

<sup>1</sup> University College of Science, Tumkur University, 572103 Tumakuru, India

<sup>2</sup> Shri Siddaganga College of Arts, Science and Commerce, 572102 Tumakuru, India

<sup>3</sup> Energy Materials Research Laboratory, Department of Chemistry,  
Siddaganga Institute of Technology, 572103 Tumakuru, India

<sup>4</sup> Department of PG Studies in Physics, Government Science College, 577501 Chitradurga, India

<sup>5</sup> Visvesvaraya Technological University, 590018 Belagavi, India

Нанокристалічні чисті та леговані Ce порошки оксиду олова (SnO<sub>2</sub>) синтезували методом горіння гелю з додаванням поверхнево-активних речовин (СТАВ і PEG), використовуючи сечовину як паливо. Підготовлені зразки характеризували PXRD, FESEM, UV-Vis, FTIR та імпедансним аналізатором. Аналіз PXRD виявив тетрагональну рутильну фазу SnO<sub>2</sub>. Розмір зерна оцінювали за допомогою рівняння Дебая-Шерпера та методу Вільямсона-Холла. Параметри елементарної комірки були знайдені за допомогою уточнення Рітвельда та графіка Нельсонса-Ріллі. На фотографіях FESEM було показано утворення наночастинок майже сферичної форми. Спектр FTIR виявив смуги завдяки фундаментальним гармонікам та комбінації з'єднань Sn-O та Sn-O-Sn. У спектрах UV-Vis показано зменшення ширини забороненої зони із вмістом Ce внаслідок збільшення дефектів. Вплив легування Ce на електричні властивості вивчали при кімнатній температурі. Діелектричні параметри  $\epsilon'$  і  $\tan\delta$  були максимальними для зразка чистого SnO<sub>2</sub>. Варіювання діелектричних властивостей та змінної провідності з частотою зумовлено міжфазною поляризацією типу Максвелла-Вагнера.

**Ключові слова:** Оксид олова, Метод горіння гелю, Уточнення Рітвельда, Змінна провідність.